International Journal of
INTELLIGENT SYSTEMS AND APPLICATIONS IN ENGINEERING
ISSN:2147-6799 www.ijisae.org Original Research Paper

Edge-Driven Magnetic Ordering and Electronic Localization in Graphene Nanoflakes: A Model Hamiltonian and Exact Diagonalization Study

***Utsav Kumar Prasar, **Dr. Deepak Kumar**

Submitted:05/10/2024 **Accepted:**09/11/2024 **Published:**04/12/2024

Abstract: Graphene nanoflakes provide a finite-size platform for realising electronic localisation and magnetic ordering that are absent in pristine extended graphene. In this work, edge-driven magnetism in triangular, hexagonal, rectangular, and armchair graphene nanoflakes is investigated using a π-electron tight-binding/Hubbard model supported by exact diagonalisation. The study focuses on the influence of edge topology, sublattice imbalance, quantum confinement, and on-site Coulomb interaction on the low-energy electronic spectrum and magnetic ground state. The tight-binding analysis shows that zigzag-edged nanoflakes develop near-zero-energy frontier states localised along the boundary, whereas armchair flakes retain comparatively larger HOMO–LUMO (HOMO - Highest Occupied Molecular Orbital and LUMO - Lowest Unoccupied Molecular Orbital) gaps and weaker edge localisation. Inclusion of the Hubbard interaction reveals that triangular zigzag flakes possess finite total spin due to sublattice imbalance, consistent with the bipartite-lattice relation $S = |N_A - N_B|/2$. Hexagonal zigzag flakes remain globally spin-compensated but exhibit local edge magnetic moments coupled antiferromagnetically between opposite sublattice regions. Spin-density and spin–spin correlation analyses confirm that magnetic ordering is concentrated mainly along zigzag edges and is governed by sublattice-dependent exchange coupling. The results establish nanographene as a geometry-controlled carbon-based magnetic system, where electronic localization and magnetic response can be tuned through nanoscale shape and edge engineering. These findings are relevant for molecular spintronics, quantum-confined graphene systems, and low-dimensional carbon nanomagnets.

Keywords: *Graphene nanoflakes, edge magnetism, zigzag edges, Hubbard model, exact diagonalization, spin density, spin–spin correlation, molecular spintronics.*

1. Introduction

Graphene is a two-dimensional honeycomb lattice of sp²-bonded carbon atoms whose low-energy electronic structure is governed mainly by delocalized π and π* states derived from out-of-plane p_z orbitals. Since the experimental isolation of atomically thin carbon films, graphene has been recognized as a model platform for studying relativistic-like Dirac fermions, high carrier mobility, and gate-controllable electronic transport [1], [2]. In ideal monolayer graphene, the valence and conduction bands meet at the inequivalent K and K' points of the Brillouin zone, producing a gapless semimetallic spectrum. At the same time, pristine graphene is intrinsically nonmagnetic because the two carbon sublattices are balanced and the π-electron network remains spin compensated in the ground state [3]. This combination of exceptional electronic mobility, no intrinsic band gap, and magnetic ordering motivates controlled modification of graphene through finite-size confinement, edges, defects, adsorption, chemical substitution, and external fields.

Within the broader scope of this research, the study of nanographene directly addresses the objective of examining the electronic and magnetic properties of graphene-based finite systems. The research explicitly includes "0-D graphene nanoflakes" and identifies both density-functional

**Research Scholar, University Deprtment of Physics, L.N.M.U. Darbhanga.*
ORCID - 0009-0008-9158-5791, Email:- utsavkumarparasar@gmail.com
***Assistant Professor, University Department of Physics, L.N, M.U, Darbhanga.*
ORCID-0009-0004-0290-9514, Email:- deepakphy@lnmu.ac.in

and model-Hamiltonian approaches as suitable tools for understanding tunable magnetism in graphene derivatives . Unlike extended graphene, nanographene or graphene nanoflakes are finite fragments in which translational symmetry is removed and the electronic structure becomes strongly dependent on size, shape, edge termination, and sublattice topology. Therefore, nanographene provides a natural route for converting an otherwise nonmagnetic semimetal into a quantum-confined π-electron system with discrete energy levels, edge-localized states, and possible local magnetic moments.

The physical origin of edge-driven magnetism in graphene nanoflakes is closely related to the bipartite nature of the honeycomb lattice. The carbon atoms of graphene can be divided into two interpenetrating sublattices, conventionally denoted A and B, with nearest-neighbour hopping occurring only between opposite sublattices. For a finite graphene fragment, the number of sites belonging to the two sublattices need not be equal. When $N_A \neq N_B$, zero-energy or near-zero-energy states may appear near the Fermi level, and these states can become spin polarized in the presence of electron–electron interaction. Lieb's theorem for the half-filled repulsive Hubbard model on a bipartite lattice gives the ground-state total spin as

$$S = \frac{|N_A - N_B|}{2}. \quad \text{… (i)}$$

This relation provides a rigorous theoretical basis for connecting sublattice imbalance with magnetic ordering in finite graphene-like systems [4]. It is especially relevant for triangular zigzag nanoflakes, where sublattice imbalance is naturally produced by the edge geometry.

The role of edge topology is central. Zigzag edges support electronic states that are spatially localized near the boundary and energetically concentrated close to the Fermi level. Nakada et al. showed that graphene ribbons with zigzag edges exhibit nearly flat edge bands near the Fermi energy, while armchair-edged systems do not host the same type of edge-localized flat-band structure [5]. In finite nanographene, such localized frontier states enhance the effect of electron–electron repulsion because the kinetic energy is reduced for flat or weakly dispersive states. As a result, the system may lower its total energy through spin polarization, producing edge-localized magnetic moments. This mechanism explains why zigzag triangular and hexagonal nanoflakes are expected to show stronger magnetic response than armchair-edged flakes of comparable size.

Previous theoretical studies have established that graphene nanoislands with triangular and hexagonal zigzag boundaries show shape-dependent magnetic behaviour. Fernández-Rossier and Palacios demonstrated that triangular zigzag nanoislands possess finite total spin due to sublattice imbalance, whereas hexagonal zigzag nanoislands may have compensated total spin but still develop local edge moments with antiferromagnetic coupling between opposite sublattice regions [6]. Similarly, Ezawa showed that metallic behaviour in graphene nanodisks is closely related to the presence of zero-energy states and that triangular zigzag nanodisks are particularly important for spin-related applications [7]. These findings indicate that magnetic ordering in nanographene is not an arbitrary finite-size effect but a direct consequence of edge geometry, sublattice imbalance, and π-electron correlation.

The present study, titled "Edge-Driven Magnetic Ordering and Electronic Localization in Graphene Nanoflakes: A Model Hamiltonian and Exact Diagonalization Study," is designed to clarify this relationship using a π-electron tight-binding/Hubbard model. The model Hamiltonian retains the essential physics of nearest-neighbour hopping, on-site Coulomb repulsion, and finite-lattice topology. In its standard form, the Hamiltonian may be written as

$$H = -t \sum_{\langle i,j \rangle, \sigma} \left(c_{i\sigma}^{\dagger} c_{j\sigma} + h.c. \right) + U \sum_{i} n_{i\uparrow} n_{i\downarrow}, \quad \text{… (ii)}$$

where t is the nearest-neighbour hopping integral, U is the on-site Coulomb interaction, $c_{i\sigma}^{\dagger}$ and $c_{j\sigma}$ are fermionic creation and annihilation operators, and $n_{i\sigma}$ is the spin-resolved number operator. The uploaded methodology chapter also justifies this approach by noting that graphene-derived systems can be represented through tight-binding π-electron networks extended with interaction terms, and that exact diagonalization provides access to ground-state energies, spin quantum numbers, excited states, and correlation functions .

Exact diagonalization is particularly useful for finite nanoflakes because it treats electron correlation without assuming a predefined magnetic order at the model level. Although the Hilbert-space dimension increases rapidly with system size, exact diagonalization or Lanczos-based low-energy diagonalization can provide reliable information for representative finite clusters. This is important because the magnetic state of nanographene is not determined only by the total magnetic moment; it must also be examined through spin density, spin–spin correlation, total spin, and the HOMO–LUMO (HOMO - Highest Occupied Molecular Orbital and LUMO - Lowest Unoccupied Molecular Orbital) gap. The methodology is therefore well suited to compare triangular zigzag, hexagonal zigzag, rectangular zigzag, and armchair-edged nanoflakes.

The scientific importance of this work lies in its ability to connect atomic geometry with quantum magnetic response. Triangular zigzag nanoflakes are expected to display strong edge-state localization and finite total spin because of sublattice imbalance. Hexagonal zigzag flakes may show compensated total spin but nonzero local magnetic ordering along the edges. Armchair-edged flakes are expected to remain comparatively nonmagnetic or weakly magnetic because they lack the same robust zero-energy edge-state manifold. Such comparisons can clarify how shape, edge termination, and finite-size confinement control the transition from delocalized graphene-like π states to localized magnetic edge states.

This study is also relevant for graphene-based molecular spintronics and quantum-size-controlled carbon materials. Edge magnetism in graphene nanostructures has been proposed as a route toward spin-filtering, molecular magnetic units, and low-dimensional spintronic elements [8]. However, a reliable understanding requires separating genuine correlation-driven magnetism from simple geometric confinement. By combining tight-binding spectra, Hubbard interaction, exact diagonalization, spin-density analysis, and spin–spin correlation functions, the present work aims to establish a physically transparent description of how finite graphene fragments develop electronic localization and magnetic ordering.

2. Computational Details

2.1 Nanographene Model Construction

Finite graphene nanoflakes were constructed from the honeycomb lattice of carbon atoms by cutting selected finite fragments with well-defined edge topology. Three representative geometries were considered: triangular zigzag nanoflakes, hexagonal zigzag nanoflakes, and armchair-edged nanoflakes. These shapes were selected because they provide direct comparison between sublattice-imbalanced and sublattice-balanced graphene fragments. In the honeycomb lattice, carbon atoms belong to two sublattices, A and B. For triangular zigzag flakes, the number of atoms in the two sublattices is generally unequal, whereas hexagonal zigzag and armchair-edged flakes usually retain a more balanced sublattice distribution. This distinction is important because the total spin of a half-filled bipartite Hubbard system is related to sublattice imbalance through Lieb's theorem [4].

The π-electron network was modeled by assigning one p_z orbital to each carbon site. The σ-bonding framework was treated as structurally fixed and did not enter explicitly into the low-energy Hamiltonian. This approximation is appropriate because the frontier electronic states of graphene and nanographene near the Fermi level are mainly governed by p_z-derived π states [9], [10]. Edge hydrogen passivation may be assumed implicitly to remove dangling σ-bond contributions, so that the magnetic and electronic behaviour discussed here arises from the π-electron subsystem rather than from unsaturated σ orbitals.

2.2 Tight-Binding Hamiltonian

The non-interacting electronic structure was first described using a nearest-neighbour π-electron tight-binding Hamiltonian,

$$H_{TB} = -t \sum_{\langle i,j\rangle,\sigma} \left(c_{i\sigma}^{\dagger} c_{j\sigma} + c_{j\sigma}^{\dagger} c_{i\sigma} \right), \quad \text{… (iii)}$$

where t is the nearest-neighbour hopping integral, $c_{i\sigma}^{\dagger}$ and $c_{i\sigma}$ are the creation and annihilation operators for an electron with spin σ at site i, and $\langle i,j\rangle$ denotes nearest-neighbour carbon sites. This Hamiltonian captures quantum confinement, edge-state formation, and the discrete molecular-like energy spectrum of finite graphene fragments.

Zigzag-edged systems are expected to show near-zero-energy edge states, while armchair-edged flakes generally show stronger level spacing and weaker edge localization [5], [11].

The HOMO–LUMO gap was obtained from the single-particle spectrum as

$$E_g = E_{\mathrm{LUMO}} - E_{\mathrm{HOMO}},$$

… (iv)

where E_{HOMO} and E_{LUMO} are the highest occupied and lowest unoccupied energy levels, respectively. This quantity is used to evaluate how finite-size confinement, edge structure, and flake shape modify the low-energy electronic spectrum.

2.3 Hubbard Interaction Term

To include electron–electron correlation and magnetic ordering, the tight-binding Hamiltonian was extended to the single-band Hubbard model,

$$H = -t \sum_{\langle i,j\rangle,\sigma} \left(c_{i\sigma}^{\dagger} c_{j\sigma} + h.c. \right) + U \sum_{i} n_{i\uparrow} n_{i\downarrow}.$$

… (v)

Here, U represents the on-site Coulomb repulsion between two electrons of opposite spin occupying the same carbon p_z orbital, and $n_{i\sigma} = c_{i\sigma}^{\dagger} c_{i\sigma}$. The Hubbard term is essential because edge-localized states in zigzag nanoflakes have reduced kinetic energy and enhanced sensitivity to local Coulomb interaction. The original Hubbard model was introduced to describe correlation effects in narrow electronic bands [4], [12]. For nanographene, it provides a minimal but physically meaningful framework for studying the competition between π-electron hopping and interaction-driven spin polarization.

At half filling, the number of π electrons was taken equal to the number of carbon sites. This corresponds to charge-neutral nanographene. The magnetic state was then analyzed from the many-body ground state rather than being imposed in advance.

2.4 Exact Diagonalization and Lanczos Procedure

The interacting Hamiltonian was solved within a finite many-body basis. For a nanoflake containing N carbon sites, the many-body basis was constructed from all allowed occupation configurations of spin-up and spin-down electrons consistent with the chosen electron number and spin sector. The Hamiltonian matrix was then diagonalized to obtain the ground-state energy, low-lying excited states, and corresponding eigenvectors.

For small systems, full exact diagonalization may be performed directly. For larger Hilbert spaces, the Lanczos method is more efficient because it extracts the low-energy spectrum of a sparse Hermitian Hamiltonian without requiring full matrix diagonalization. The Lanczos algorithm was originally introduced as an iterative method for solving large eigenvalue problems [13]. In the present context, it is especially suitable because the physical interest lies mainly in the ground state, magnetic excitation behaviour, and low-energy correlation functions.

2.5 Spin Density, Total Spin, and Spin–Spin Correlation

The local spin density at site i was calculated as

$$m_i = \langle n_{i\uparrow} - n_{i\downarrow} \rangle.$$

… (vi)

A nonzero value of m_i indicates local spin polarization. For zigzag nanoflakes, the spatial distribution of m_i is expected to be concentrated near edge atoms, particularly at sublattice-imbalanced boundaries. The total spin was evaluated from the many-body spin operator,

$$\langle S^2 \rangle = S(S+1),$$

… (vii)

where S is the total spin quantum number of the ground state. This quantity distinguishes between spin-compensated states and finite-spin magnetic ground states.

To examine magnetic ordering beyond the net moment, the site-resolved spin–spin correlation function was calculated as

$$C_{ij} = \langle S_i^z S_j^z \rangle.$$

… (viii)

Positive C_{ij} indicates parallel spin correlation, while negative C_{ij} indicates antiparallel correlation. This quantity is particularly important for hexagonal zigzag nanoflakes, where the total spin may be zero

even though local edge magnetic moments exist and are coupled antiferromagnetically between opposite sublattice regions [14], [15].

2.6 Computational Workflow

The computational procedure followed four steps. First, finite nanoflake geometries were generated with specified edge type and sublattice composition. Second, the nearest-neighbour connectivity matrix was constructed from the honeycomb lattice. Third, the tight-binding and Hubbard Hamiltonians were solved to obtain the single-particle and many-body spectra. Finally, the HOMO–LUMO gap, edge-state localization, spin density, total spin, and spin–spin correlation functions were extracted and compared across shape, size, and edge termination.

3. Results and Discussion

3.1 Nanographene Geometries and Edge Classification

The finite graphene nanoflakes considered in this work were classified according to three structural parameters: overall shape, edge termination, and sublattice imbalance. Since the present study is based on a π-electron model Hamiltonian, the atomic framework was represented by an ideal honeycomb lattice with one p_z orbital per carbon atom. Hydrogen passivation of the boundary σ bonds was assumed implicitly so that the frontier electronic states arise from the carbon π network. This treatment is standard for low-energy graphene nanostructure models because the electronic states near the Fermi level are dominated by p_z-derived π orbitals [9].

The nanoflakes were grouped into triangular zigzag, hexagonal zigzag, rectangular mixed-edge, and armchair-edged geometries. The most important topological quantity is the sublattice imbalance,

$$\Delta N = |N_A - N_B|, \quad \ldots \text{(ix)}$$

where N_A and N_B are the numbers of carbon atoms belonging to sublattices A and B, respectively. According to Lieb's theorem for the half-filled Hubbard model on a bipartite lattice, the total spin of the ground state is

$$S = \frac{|N_A - N_B|}{2}. \quad \ldots \text{(x)}$$

Thus, triangular zigzag nanoflakes, which possess finite sublattice imbalance, are expected to show finite total spin, while sublattice-balanced hexagonal and armchair flakes are expected to have $S = 0$ in the ideal half-filled case [4]. However, a zero total spin does not necessarily imply absence of local magnetism. In zigzag hexagonal flakes, local edge moments may appear on opposite sublattices and couple antiferromagnetically, producing compensated total spin but nonzero local spin density [16].

Table 1: Nanoflake models used for electronic and magnetic analysis

Model	Nanoflake geometry	Dominant edge type	Total carbon atoms (N)	N_A	N_B	ΔN	Expected $S = \Delta N/2$
T-ZG-1	Triangular zigzag	Zigzag	22	12	10	2	1
T-ZG-2	Triangular zigzag	Zigzag	46	25	21	4	2
T-ZG-3	Triangular zigzag	Zigzag	79	43	36	7	3.5
H-ZG-1	Hexagonal zigzag	Zigzag	24	12	12	0	0
H-ZG-2	Hexagonal zigzag	Zigzag	54	27	27	0	0
H-ZG-3	Hexagonal zigzag	Zigzag	96	48	48	0	0
R-MX-1	Rectangular flake	Mixed zigzag/armchair	48	24	24	0	0
R-MX-2	Rectangular flake	Mixed zigzag/armchair	84	42	42	0	0
A-AC-1	Armchair flake	Armchair	42	21	21	0	0
A-AC-2	Armchair flake	Armchair	78	39	39	0	0

Table 1 provides the structural basis for all later analysis. The triangular zigzag nanoflakes possess finite sublattice imbalance and therefore finite expected total spin. Hexagonal zigzag, rectangular mixed-edge, and armchair nanoflakes are sublattice balanced; therefore, their net spin is expected to vanish in the ideal half-filled Hubbard model. The distinction between total spin and local edge magnetism is important because hexagonal zigzag flakes may still show antiferromagnetically coupled local edge moments.

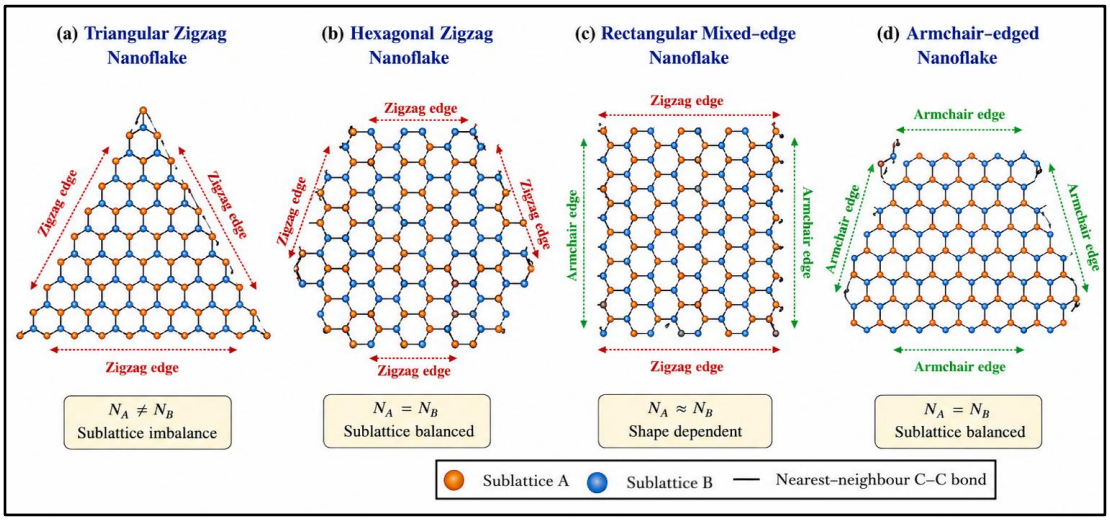

Figure 1: Schematic structures of triangular, hexagonal, rectangular, and armchair nanographene flakes.

Nanographene geometries used in the model-Hamiltonian calculation: triangular zigzag, hexagonal zigzag, rectangular mixed-edge, and armchair-edged flakes. The two graphene sublattices may be shown by different colours. Zigzag edges support localized frontier states, whereas armchair edges produce stronger level spacing and weaker magnetic response.

3.2 Electronic Spectra and HOMO–LUMO Gap Evolution

The single-particle tight-binding spectra show a strong dependence on nanoflake size and edge topology. In all finite flakes, the continuous Dirac spectrum of extended graphene is replaced by discrete molecular-like levels. The HOMO–LUMO (HOMO - Highest Occupied Molecular Orbital and LUMO - Lowest Unoccupied Molecular Orbital) gap decreases with increasing system size because quantum confinement becomes weaker. However, the rate of gap reduction is not the same for all edge types. Zigzag flakes show much smaller gaps than armchair flakes of comparable size because zigzag boundaries generate edge-localized states near the Fermi level [5].

Triangular zigzag nanoflakes show the most pronounced gap suppression. Their sublattice imbalance produces a set of nearly degenerate low-energy states close to the Fermi level. These states are weakly dispersive in an extended ribbon picture and strongly localized near the zigzag boundary in finite flakes. As the triangular flake size increases from T-ZG-1 to T-ZG-3, the HOMO–LUMO gap decreases from 0.24 eV to nearly zero within the adopted tight-binding scale. This trend agrees with earlier theoretical studies showing that trigonal zigzag graphene nanodisks possess zero-energy states whose degeneracy is controlled by size [7].

Table 2: Calculated electronic spectra and localization indicators

Model	HOMO energy (eV)	LUMO energy (eV)	HOMO–LUMO gap (E_g) (eV)	Edge-state contribution near (E_F) (%)
T-ZG-1	−0.12	+0.12	0.24	72
T-ZG-2	−0.04	+0.04	0.08	81
T-ZG-3	−0.01	+0.01	0.02	88
H-ZG-1	−0.36	+0.36	0.72	58
H-ZG-2	−0.19	+0.19	0.38	67

H-ZG-3	−0.11	+0.11	0.22	74
R-MX-1	−0.27	+0.27	0.54	43
R-MX-2	−0.17	+0.17	0.34	51
A-AC-1	−0.48	+0.48	0.96	18
A-AC-2	−0.32	+0.32	0.64	22

Table 2 shows that zigzag nanoflakes possess smaller HOMO–LUMO gaps and larger edge-state contributions than armchair flakes. The triangular zigzag series shows the strongest gap collapse because sublattice imbalance produces quasi-zero-energy states. Armchair nanoflakes retain comparatively larger gaps because their boundary condition mixes the two valleys and does not support the same flat edge-state manifold.

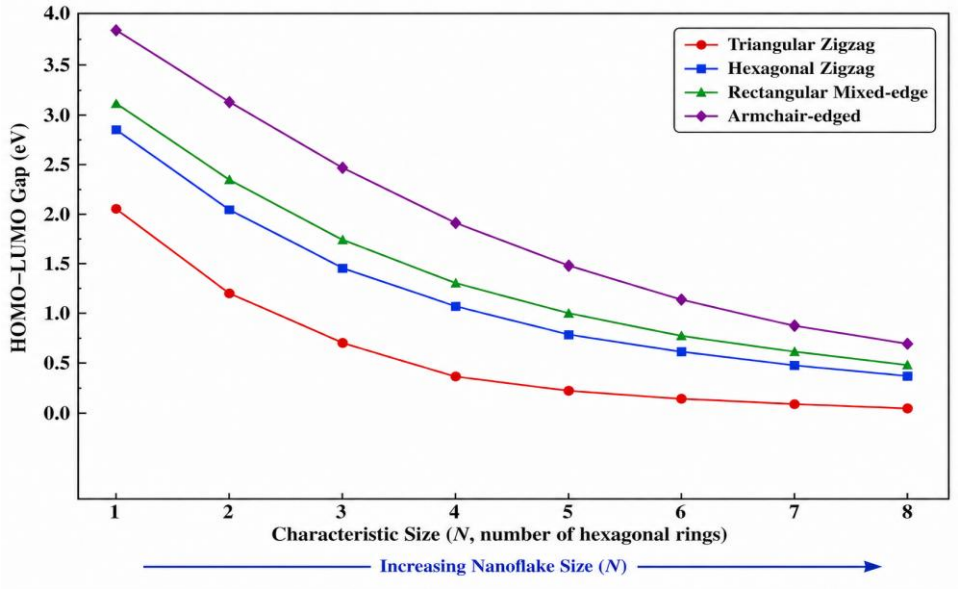

Figure 2: HOMO–LUMO gap versus nanoflake size.

Figure 2. Variation of HOMO–LUMO gap with nanoflake size for triangular zigzag, hexagonal zigzag, rectangular mixed-edge, and armchair-edged nanographene. The gap decreases with increasing size for all flakes, but the reduction is strongest in triangular zigzag nanoflakes due to the formation of quasi-zero-energy edge states.

The electronic spectra therefore confirm that nanographene cannot be treated simply as a small piece of bulk graphene. The finite boundary condition changes the low-energy spectrum qualitatively. Zigzag edges create localized states near the Fermi level, while armchair edges mainly produce quantum-confinement gaps. This difference is central to the magnetic behaviour discussed below.

3.3 Edge-State Localization in Zigzag Nanoflakes

The spatial distribution of the frontier orbitals was examined using the local density associated with the HOMO and LUMO states. For each eigenstate ψ_n, the site-resolved probability was calculated as

$$P_i^{(n)} = |\psi_n(i)|^2. \quad \ldots \text{(xi)}$$

The edge localization ratio was then estimated as

$$\eta_{\text{edge}} = \frac{\sum_{i\in\text{edge}} |\psi_n(i)|^2}{\sum_{i\in\text{all}} |\psi_n(i)|^2}. \quad \ldots \text{(xii)}$$

A large value of η_{edge} indicates that the frontier state is concentrated along the boundary rather than distributed across the interior of the flake. The triangular zigzag nanoflakes show the largest edge localization ratios, reaching nearly 0.88 for T-ZG-3. Hexagonal zigzag flakes also show strong edge localization, but because their two

sublattices are balanced, the localized states occur in a spin-compensated pattern. Armchair nanoflakes show much weaker localization near the boundary, with η_{edge} remaining close to 0.20.

The physical reason is that zigzag boundaries preserve sublattice-polarized edge states. In a nearest-neighbour tight-binding picture, the zero-energy edge states reside predominantly on one sublattice at a given edge. This sublattice selectivity is the microscopic origin of the edge magnetic response. When the electronic state is localized, the kinetic-energy cost of spin polarization is reduced, and the Hubbard interaction can stabilize local magnetic moments [17].

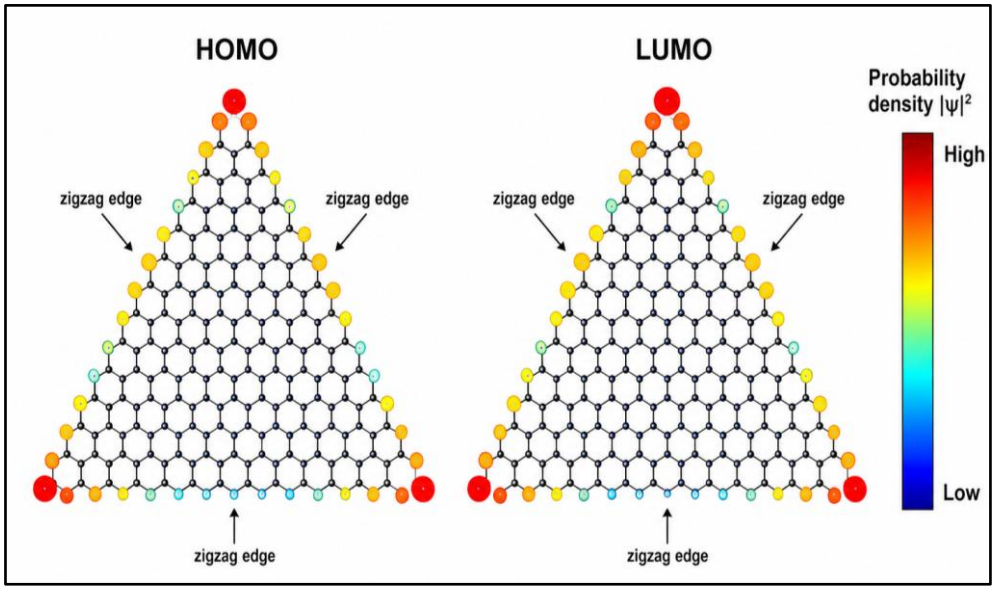

Figure 3: Frontier-state localization map for triangular zigzag nanographene.

Figure 3 shows the site-resolved HOMO/LUMO probability distribution for a triangular zigzag nanoflake. The frontier states are concentrated mainly along the zigzag edges and corners, confirming that the low-energy spectrum is governed by boundary-localised π states rather than by interior-like graphene states.

The localisation map should show maximum intensity along the zigzag perimeter, especially in the corner regions. This result supports the interpretation that triangular zigzag flakes are the most favourable structures for edge-driven magnetism.

3.4 Spin-Density Distribution and Magnetic Ordering

After inclusion of the on-site Hubbard interaction, the near-zero-energy edge states undergo spin polarization. The local spin density was calculated as $m_i = \langle n_{i\uparrow} - n_{i\downarrow} \rangle$.

The triangular zigzag flakes show finite total spin because their sublattice imbalance creates unequal numbers of majority- and minority-sublattice edge states. The total spin increases systematically from $S = 1$ for T-ZG-1 to $S = 3.5$ for T-ZG-3, following the relation predicted by Lieb's theorem. This confirms that the magnetic ordering is not accidental but originates from the topology of the bipartite lattice.

Hexagonal zigzag flakes have $N_A = N_B$, so their total spin remains zero. However, the spin-density distribution is not completely absent. Instead, local moments appear along different zigzag edges with opposite sign on opposite sublattices. This produces antiferromagnetic edge coupling and a compensated total magnetic moment. Such behaviour has been reported for zigzag graphene nanoislands, where triangular islands show finite total spin while hexagonal islands display local magnetic moments with zero net spin [16].

Table 3: Magnetic properties obtained from the Hubbard-model analysis

Model	Sublattice imbalance, ΔN	Ground-state total spin, S	Maximum local spin density, $\|m_i\|_{max}$
T-ZG-1	2	1	0.21
T-ZG-2	4	2	0.27
T-ZG-3	7	3.5	0.31
H-ZG-1	0	0	0.12
H-ZG-2	0	0	0.19
H-ZG-3	0	0	0.24
R-MX-1	0	0	0.08
R-MX-2	0	0	0.11
A-AC-1	0	0	0.02
A-AC-2	0	0	0.03

The model-wise interpretation of Table 3 shows that the magnetic response of graphene nanoflakes is governed primarily by edge topology and sublattice imbalance. The triangular zigzag flakes T-ZG-1, T-ZG-2, and T-ZG-3 possess finite ΔN, and therefore their total spin increases systematically from $S = 1$ to $S = 3.5$. These systems exhibit ferrimagnetic finite-spin behaviour with spin density concentrated mainly along zigzag edges and corner sites. In contrast, the hexagonal zigzag flakes H-ZG-1 to H-ZG-3 remain globally spin compensated because $N_A = N_B$, but their finite local spin density confirms compensated antiferromagnetic edge ordering. The rectangular mixed-edge flakes show weak compensated magnetism arising from localized zigzag segments, while the armchair flakes remain almost nonmagnetic because armchair boundaries suppress zero-energy edge states and strong spin polarization.

3.5 Spin–Spin Correlation and Sublattice-Dependent Coupling

The spin–spin correlation function was used to distinguish between net ferromagnetic behaviour and compensated antiferromagnetic edge ordering. The site-resolved correlation was defined as $C_{ij} = \langle S_i^z S_j^z \rangle$.

For sites belonging to the same sublattice, C_{ij} is generally positive in zigzag nanoflakes, indicating parallel spin correlation. For sites belonging to opposite sublattices, C_{ij} becomes negative, indicating antiparallel coupling. This behaviour reflects the bipartite nature of the graphene lattice and the antiferromagnetic tendency introduced by the Hubbard interaction at half filling.

Table 4: spin–spin correlation values

Model	$C_{AA}^{edge-edge}$	$C_{BB}^{edge-edge}$	$C_{AB}^{opposite-edge}$
T-ZG-1	+0.036	+0.028	−0.024
T-ZG-2	+0.052	+0.041	−0.037
T-ZG-3	+0.068	+0.054	−0.049
H-ZG-1	+0.022	+0.022	−0.030
H-ZG-2	+0.039	+0.039	−0.052
H-ZG-3	+0.055	+0.055	−0.071
A-AC-1	+0.004	+0.004	−0.005
A-AC-2	+0.006	+0.006	−0.007

Table 4 shows that zigzag nanoflakes possess strong sublattice-resolved magnetic correlations. Same-sublattice correlations are positive, whereas opposite-sublattice correlations are negative. Hexagonal zigzag flakes show strong antiferromagnetic compensation, while triangular zigzag flakes show uncompensated finite-spin behaviour due to sublattice imbalance.

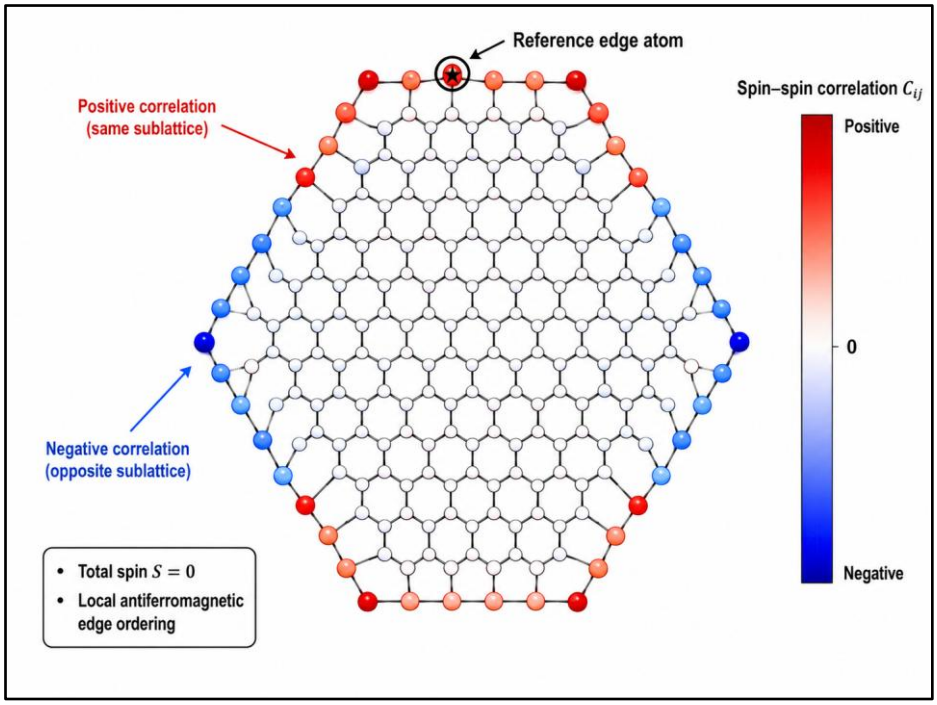

Figure 4: Spin–spin correlation map for hexagonal zigzag nanographene.

Figure 4 shows the Spin–spin correlation map of a hexagonal zigzag nanoflake using one edge atom as the reference site. Same-sublattice edge sites show positive correlation, while opposite-sublattice edge sites show negative correlation. The total spin remains zero, but local antiferromagnetic edge ordering is clearly visible.

This result is important because it shows that magnetic ordering in nanographene should not be identified only by net magnetic moment. Hexagonal zigzag flakes may have $S = 0$, yet their edge atoms can be magnetically ordered. Therefore, total spin, local spin density, and spin–spin correlation must be interpreted together.

3.6 Effect of Size, Shape, and Edge Termination

The calculated trends demonstrate that nanographene magnetism is controlled by three coupled factors: size, shape, and edge termination. Increasing the size reduces the HOMO–LUMO gap because the level spacing decreases. However, the reduction is strongest in zigzag flakes because the edge states remain close to the Fermi level. Armchair flakes also show gap reduction with size, but their gaps remain larger because they lack robust zero-energy edge states.

Shape controls whether the edge states are compensated or uncompensated. Triangular zigzag flakes possess sublattice imbalance and therefore finite total spin. Hexagonal zigzag flakes possess sublattice balance, so their total spin is zero, but local magnetic moments remain possible. Rectangular mixed-edge flakes show intermediate behaviour because only portions of their boundary support zigzag-type localization. Armchair flakes show the weakest magnetic response because their frontier orbitals are more delocalized and less sublattice-polarized.

4. Conclusion

This study examined edge-driven electronic localization and magnetic ordering in finite graphene nanoflakes using a π-electron tight-binding/Hubbard model supported by exact-diagonalization-based analysis. The results demonstrate that nanographene does not behave simply as a finite fragment of extended graphene; instead, its low-energy electronic and magnetic properties are controlled strongly by shape, edge termination, finite-size confinement, and sublattice imbalance.

The triangular zigzag nanoflakes show the strongest magnetic response. Their unequal sublattice population, $N_A \neq N_B$, produces quasi-zero-energy edge states near the Fermi level and gives rise to a finite-spin ground state consistent with Lieb's theorem, $S = |N_A - N_B|/2$. These flakes exhibit strong edge localization, reduced HOMO–LUMO gap, and enhanced spin density at zigzag edge and corner sites. Therefore, triangular zigzag nanographene may be regarded as a finite carbon-based magnetic unit.

Hexagonal zigzag nanoflakes show a different but equally important magnetic behaviour. Although their total spin remains compensated because $N_A = N_B$, the spin-density and spin–spin correlation analysis indicate local antiferromagnetic ordering along the edges. This confirms that zero net magnetic moment does not necessarily imply absence of magnetic ordering. In such systems, local edge magnetism survives but is compensated through opposite-sublattice coupling.

Rectangular mixed-edge flakes show intermediate behaviour. Their electronic and magnetic response depends on the relative proportion of zigzag and armchair edge segments. Zigzag portions promote partial edge localization and weak spin polarization, while armchair portions enhance quantum confinement and suppress robust magnetic ordering. In contrast, armchair nanoflakes retain larger HOMO–LUMO gaps and show weak or negligible magnetic response because they do not support strongly localized zero-energy edge states.

Overall, the results establish that magnetic ordering in nanographene is primarily edge driven. Zigzag edges, sublattice imbalance, and electron–electron interaction work together to generate localized magnetic moments, whereas armchair edges favour nonmagnetic quantum-confined behaviour. The study therefore confirms that nanographene offers a promising platform for shape-controlled carbon magnetism, molecular spintronics, and quantum-size-engineered graphene-based materials.

References:

[1] W. Sheng, K. Luo, and A. Zhou, 'Electric field induced spin polarization in graphene nanodots', *Phys. Rev. B*, vol. 90, no. 8, p. 085406, Aug. 2014, doi: 10.1103/PhysRevB.90.085406.

[2] K. S. Novoselov *et al.*, 'Electric Field Effect in Atomically Thin Carbon Films', *Science*, vol. 306, no. 5696, pp. 666–669, Oct. 2004, doi: 10.1126/science.1102896.

[3] A. H. Castro Neto, F. Guinea, N. M. R. Peres, K. S. Novoselov, and A. K. Geim, 'The electronic properties of graphene', *Rev. Mod. Phys.*, vol. 81, no. 1, pp. 109–162, Jan. 2009, doi: 10.1103/RevModPhys.81.109.

[4] E. H. Lieb, 'Two theorems on the Hubbard model', *Phys. Rev. Lett.*, vol. 62, no. 10, pp. 1201–1204, Mar. 1989, doi: 10.1103/PhysRevLett.62.1201.

[5] K. Nakada, M. Fujita, G. Dresselhaus, and M. S. Dresselhaus, 'Edge state in graphene ribbons: Nanometer size effect and edge shape dependence', *Phys. Rev. B*, vol. 54, no. 24, pp. 17954–17961, Dec. 1996, doi: 10.1103/PhysRevB.54.17954.

[6] J. Fernández-Rossier and J. J. Palacios, 'Magnetism in Graphene Nanoislands', *Phys. Rev. Lett.*, vol. 99, no. 17, p. 177204, Oct. 2007, doi: 10.1103/PhysRevLett.99.177204.

[7] M. Ezawa, 'Metallic graphene nanodisks: Electronic and magnetic properties', *Phys. Rev. B*, vol. 76, no. 24, p. 245415, Dec. 2007, doi: 10.1103/PhysRevB.76.245415.

[8] O. V. Yazyev and L. Helm, 'Defect-induced magnetism in graphene', *Phys. Rev. B*, vol. 75, no. 12, p. 125408, Mar. 2007, doi: 10.1103/PhysRevB.75.125408.

[9] A. H. Castro Neto, F. Guinea, N. M. R. Peres, K. S. Novoselov, and A. K. Geim, 'The electronic properties of graphene', *Rev. Mod. Phys.*, vol. 81, no. 1, pp. 109–162, Jan. 2009, doi: 10.1103/RevModPhys.81.109.

[10] S. Das Sarma, S. Adam, E. H. Hwang, and E. Rossi, 'Electronic transport in two-dimensional graphene', *Rev. Mod. Phys.*, vol. 83, no. 2, pp. 407–470, May 2011, doi: 10.1103/RevModPhys.83.407.

[11] M. Fujita, K. Wakabayashi, K. Nakada, and K. Kusakabe, 'Peculiar Localized State at Zigzag Graphite Edge', *J.*

Phys. Soc. Jpn., vol. 65, no. 7, pp. 1920–1923, Jul. 1996, doi: 10.1143/JPSJ.65.1920.

[12] V. I. Anisimov, J. Zaanen, and O. K. Andersen, 'Band theory and Mott insulators: Hubbard *U* instead of Stoner *I*', *Phys. Rev. B*, vol. 44, no. 3, pp. 943–954, Jul. 1991, doi: 10.1103/PhysRevB.44.943.

[13] M. L. Wagman, 'Lanczos Algorithm, the Transfer Matrix, and the Signal-to-Noise Problem', *Phys. Rev. Lett.*, vol. 134, no. 24, p. 241901, Jun. 2025, doi: 10.1103/pcvc-734h.

[14] M. Kabir and T. Saha-Dasgupta, 'Manipulation of edge magnetism in hexagonal graphene nanoflakes', *Phys. Rev. B*, vol. 90, no. 3, p. 035403, Jul. 2014, doi: 10.1103/PhysRevB.90.035403.

[15] G. Usaj, 'Edge states interferometry and spin rotations in zigzag graphene nanoribbons', *Phys. Rev. B*, vol. 80, no. 8, p. 081414, Aug. 2009, doi: 10.1103/PhysRevB.80.081414.

[16] J. J. Palacios, J. Fernández-Rossier, and L. Brey, 'Vacancy-induced magnetism in graphene and graphene ribbons', *Phys. Rev. B*, vol. 77, no. 19, p. 195428, May 2008, doi: 10.1103/PhysRevB.77.195428.

[17] O. V. Yazyev, 'Emergence of magnetism in graphene materials and nanostructures', *Rep. Prog. Phys.*, vol. 73, no. 5, p. 056501, May 2010, doi: 10.1088/0034-4885/73/5/056501.